NEAR FIELD AND REGIONAL MODELING OF EXPLOSIONS AT THE DEGELEN TEST SITE

J. L. Stevens[1], N. Rimer[1], H. Xu[1], J. R. Murphy[1], G. E. Baker[1]
G. G. Kocharyan[2], B. A. Ivanov[2], and S.M. Day[3]

[1]Science Applications International Corporation
[2]Institute for the Dynamics of the Geospheres
[3] San Diego State University

ABSTRACT

The objective of this research program is to improve the capability to predict the seismic source characteristics of underground explosions in rock. This is being accomplished by development of improved dynamic failure models that are constrained by a large unique data set of near-field waveforms and parametric data from both U.S. tests and historic Soviet explosions at the Degelen Test Site. In addition, we are analyzing regional seismic data along a seismic line located north of the Degelen Test Site that recorded data at 9 stations spaced approximately evenly from the test site to a distance of about 100 km. This project is a collaborative effort between SAIC and the Russian Institute for the Dynamics of the Geospheres (IDG).

IDG is in the process of digitizing data from 25 nuclear tests at Degelen. The complete data set consists of 81 near-field waveforms recorded underground at shot depth and 124 near-regional seismic records. Most seismic records include both a vertical and radial waveform. This data set provides a rare opportunity to observe and model the seismic wavefield of the explosions as they evolve from the near field of the explosion out to regional distances. To date, IDG has digitized 27 near-field waveforms and 122 seismic waveforms. We are in the process of defining the optimum procedures to model this data. The goal is to develop material models that are consistent with the data and have a realistic physical basis. Work to date at SAIC has focused on implementation and testing of improved numerical modeling procedures and simulation of near-regional data. We are testing acoustic fluidization as a physical mechanism for strength reduction in nonlinear explosion simulations. Near regional data is being modeled using wave number integration. We are also comparing the Degelen data with similar data from NTS explosions. The near-field Degelen data received to date is lower in amplitude than would be predicted based on NTS experience. Although both the NTS explosions being reviewed and the Degelen explosions were in granite, the material properties of the rock are significantly different. The most significant difference is higher porosity in the Degelen granite. The data set of near-field and regional waveforms will be delivered to the Center for Monitoring Research upon completion of this project.

KEY WORDS: rock mechanics, Degelen, explosion, numerical modeling

1. REPORT DATE **OCT 2001**	2. REPORT TYPE	3. DATES COVERED **00-00-2001 to 00-00-2001**

4. TITLE AND SUBTITLE	5a. CONTRACT NUMBER
Near Field And Regional Modeling Of Explosions At The Degelen Test Site	5b. GRANT NUMBER
	5c. PROGRAM ELEMENT NUMBER
6. AUTHOR(S)	5d. PROJECT NUMBER
	5e. TASK NUMBER
	5f. WORK UNIT NUMBER

7. PERFORMING ORGANIZATION NAME(S) AND ADDRESS(ES) **Science Applications International Corporation,10260 Campus Point Drive,San Diego,CA,92121**	8. PERFORMING ORGANIZATION REPORT NUMBER

9. SPONSORING/MONITORING AGENCY NAME(S) AND ADDRESS(ES)	10. SPONSOR/MONITOR'S ACRONYM(S)
	11. SPONSOR/MONITOR'S REPORT NUMBER(S)

12. DISTRIBUTION/AVAILABILITY STATEMENT
Approved for public release; distribution unlimited

13. SUPPLEMENTARY NOTES
Proceedings of the 23rd Seismic Research Review: Worldwide Monitoring of Nuclear Explosions held in Jackson Hole, WY on 2-5 of October, 2001. U.S. Government or Federal Rights.

14. ABSTRACT
See Report

15. SUBJECT TERMS

16. SECURITY CLASSIFICATION OF:			17. LIMITATION OF ABSTRACT	18. NUMBER OF PAGES	19a. NAME OF RESPONSIBLE PERSON
a. REPORT **unclassified**	b. ABSTRACT **unclassified**	c. THIS PAGE **unclassified**	**Same as Report (SAR)**	**10**	

OBJECTIVE

The main objective of this research program is to improve the capability to predict the seismic source characteristics of underground explosions in rock. This is being accomplished by development of improved dynamic failure models for hardrock that are constrained by a large unique data set of near-field waveforms and parametric data from both U.S. tests and historic Soviet explosions at the Degelen Test Site. In addition, we are analyzing regional seismic data along a seismic line located north of the Degelen Test Site that recorded data at 9 stations spaced approximately evenly from the test site to a distance of about 100 km. This project is a collaborative effort between SAIC and the Russian Institute for the Dynamics of the Geospheres (IDG).

RESEARCH ACCOMPLISHED

Introduction

Empirical and numerical models of explosion sources do a fairly good job of matching observed seismic signals, but the physical basis for the explosion source is still not well understood. In particular, numerical models of explosion sources developed using laboratory measurements of rock properties predict particle velocity pulse widths that are roughly a factor of 3-5 smaller than those observed near field in hardrock events such as PILEDRIVER. The basic problem is that the strength of the rock measured in the laboratory is much larger than the apparent strength of the rock as determined from the near field ground motion.

A number of solutions to these problems have been proposed over the years, including the effective stress model (Rimer, et al, 1984), and various types of damage models. These models all have the characteristic that the material strength is reduced dynamically to a very low level when the rock fails. The effective stress model says that the weakness comes from water within the rock matrix, and that the broken rock in effect floats on water that is squeezed out of pores or fractures when the rock fails. Although there are questions about the realism of this physical model, it works fairly well to explain the near field waveforms. Figure 1 shows a comparison of the PILEDRIVER waveforms with waveforms calculated using the effective stress model. The agreement is quite good, particularly at the closer two stations. Furthermore, when the PILEDRIVER solution was scaled to the appropriate yield and compared with other US explosions in granite (Hardhat and Shoal), agreement with the observed waveforms was also quite good (Stevens, et al, 1986).
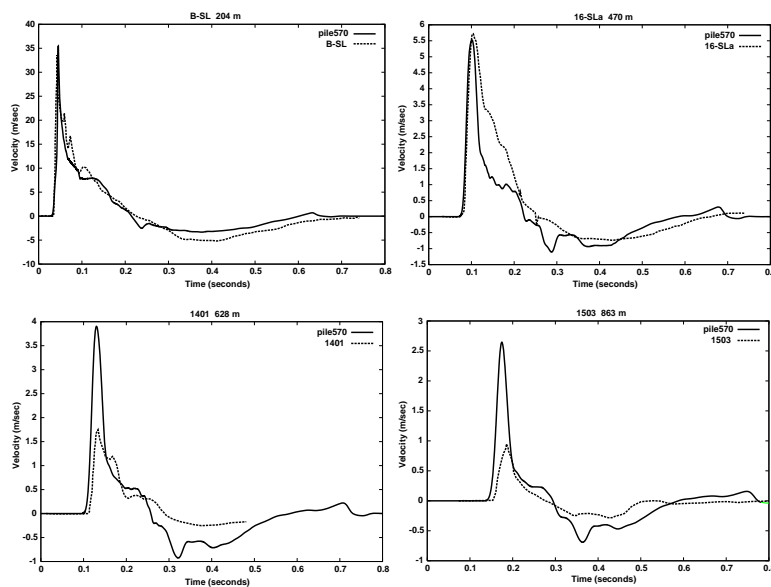

Figure 1. Particle velocity measurements at working point depth from PILEDRIVER compared to numerical simulation pile570 using the effective stress law.

Under a previous DTRA contract, SAIC (at the time Maxwell Technologies) worked together with the IDG and the University of Southern California (USC) to develop improved material models. IDG provided extensive measurements of material properties close to nuclear and chemical explosions both before and after the explosions were detonated (Rimer, et al, 1998). In addition, we implemented the micro-mechanical damage mechanics model for the growth and coalescence of cracks in brittle rocks under compressive loading which was developed by Prof. Charles Sammis of USC into SAIC's nonlinear finite difference codes and then used this model to simulate the observed explosion damage and a small set of near field waveforms that were also provided by IDG. The results of this work are discussed in detail in the final report (Rimer et al, 1999). Since the Sammis damage model does not predict what happens to the rock after unstable brittle failure occurs, the calculations introduced a friction law model post-failure. However, realistic values of friction did not provide enough strength reduction to match the near field data. We were more successful in matching the data by dropping the coefficient of friction to very low values (as low as 0.02) for rubbleized rock, but this again leaves the question of what physical mechanism could be responsible for these very low values and corresponding low strength.

A possible answer initially proposed by Melosh (1979) is "acoustic fluidization". The physics behind this mechanism is that there is a complex dynamic acoustic wavefield that causes high frequency vibrations in the broken rock. These vibrations cause rapidly changing regions of high and low normal stress, and remove the frictional normal stress from parts of the rock as it moves. Consequently parts of the rock are not confined by the frictional stress and in effect have much lower strength. Acoustic fluidization has been used to explain other phenomena such as landslides and craters (Melosh and Ivanov, 1999), which have been similarly difficult to explain because of anomalously low apparent friction. Initial efforts to include acoustic fluidization in our numerical models are described later in this paper.

Degelen Near Field and Near Regional Seismic Data

The numerical modeling component of this project is being constrained by a much better data set than has been available in the past. Near field waveforms are only available from a small number of U.S. nuclear tests, and until recently, none have been available from the testing program of the former Soviet Union. IDG has near field records from a number of nuclear explosions at the Degelen test site that are being digitized for this project. IDG will also be providing near source material properties measurements from these events. In addition, IDG has data from a seismic line located north of the Degelen test site that was maintained with consistent instrumentation for many years during the Soviet testing program. Figure 2 shows a map illustrating the location of the test sites and the seismic stations.
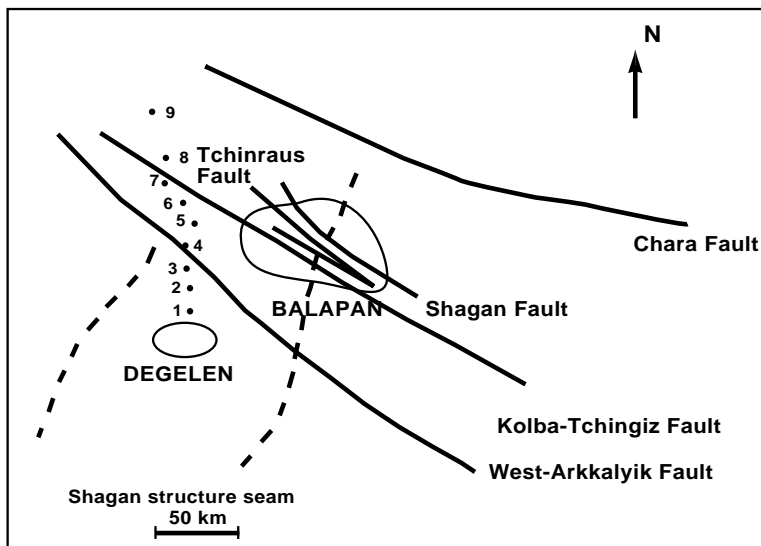

Figure 2. Map showing the locations of the former Soviet Degelen and Balapan test sites, faults, and seismic stations in the region.

The 9 seismic stations are spread out at approximately even intervals from the Degelen test site out to a distance of about 100 km. IDG is also digitizing seismic data from these stations for all of the events that have near field records. This provides a rare opportunity to observe and model the seismic wavefield of the explosions as they evolve from the near field of the explosion out to regional distances. The data that IDG has identified for digitization, and the data digitized as of this writing are listed in Table 1. Figure 3 shows waveforms from one of these explosions.

Table 1. Degelen events with near field and/or seismic records, and waveforms digitized to date. (The total number of digitized records including multiple recordings at some stations, are shown in parentheses. Explosion yield and ISC m_b are shown for events digitized to date.)

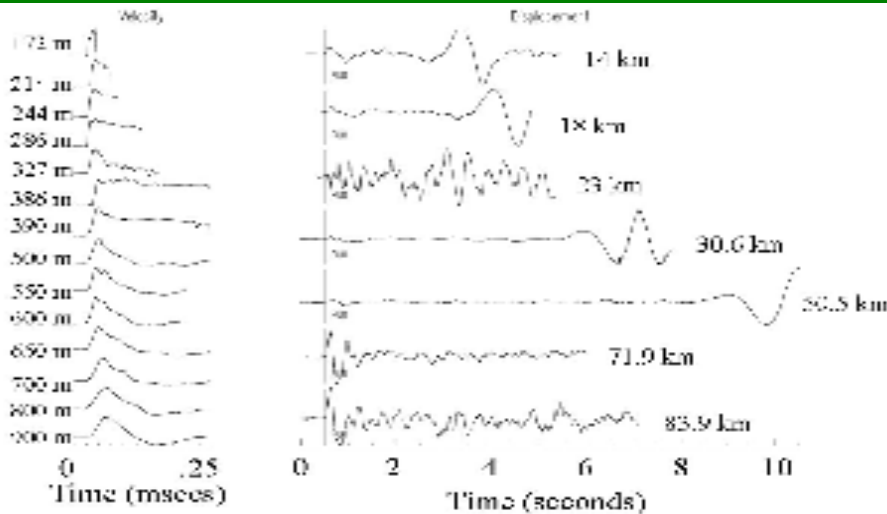| Date	Yield (Kt)	m_b	Number of near field records	Waveforms Digitized	Distance range, m	Number of seismic records	Waveforms Digitized	Distance range, km
1988/04/22	2.3	4.9	2	2	69-183	3	3	57-81
1988/11/23	19	5.4	4	3	280-475	9	9	14-83
1987/07/17	78	5.8	14	14	170-900	7	7	14.5-84
1987/10/16	1.1	4.6	4	4	55-132	8	8 (27)	20-76
1989/10/04	1.8	4.7	4	4 (5)	45-285	8	8 (24)	16-85
1981/07/17	9.3	5.1	3	3	115-310	8	8 (27)	15-80
1965/02/04	.001-20	-	4	4	147-750	9	peaks	14-83
1964/05/16	20-150	6.2	4	4	150-600	9	peaks	13-80
1966/03/20			4		300-600	9		15-84
1966/02/13			4		350-600	9		14-80
1973/12/31			4		110-230			
1974/12/16			4		100-200			
1978/03/26			5		76-270			
1980/06/25			3		155-310			
1982/12/25			4		90-190			
1984/10/18			4		35-110			
1968/07/12			2		80-90			
1968/12/18			3		200-510			
1970/06/28			2		200-240			
1980/09/25			3		100-160			
1971/12/15						9		7.5-85
1987/05/06						9		13-83
1987/12/20						9		13-83
1988/10/18						9		11-77
1989/02/17						9		10-77

Figure 3. Near-field (left) and near regional seismic (right) waveforms from the 1987/07/17 event.

The near field records in Figure 3 show the evolution of the waveform from the nonlinear to linear regions. Unfortunately, the absolute times are not known for the records. The near regional records show the evolution of the waveform from 14 to 83 km. A strong Rg phase is present in several seismograms that persists to quite a long distance. Some of the records end before the start of the Rg phase and therefore do

543

not show it. Figure 4 shows a comparison of synthetic and observed seismograms for three of the near regional waveforms from the 1987/07/17 event. The synthetic seismograms were constructed using wavenumber integration (Luco and Apsel, 1983) using the East Kazakh structure from Stevens (1986). The synthetic seismograms were low-pass filtered at 2 Hz. The persistence of Rg calls into question the explanation of Rg scattering as the source of Lg since that mechanism requires most of Rg to scatter into Lg within a few kilometers of the source.

Figure 5 shows a comparison between peak velocity measurements from the first three explosions listed in Table 1 and peak velocity measurements from other explosions in granite. The Degelen velocities are near the lower bound of the other velocity measurements.
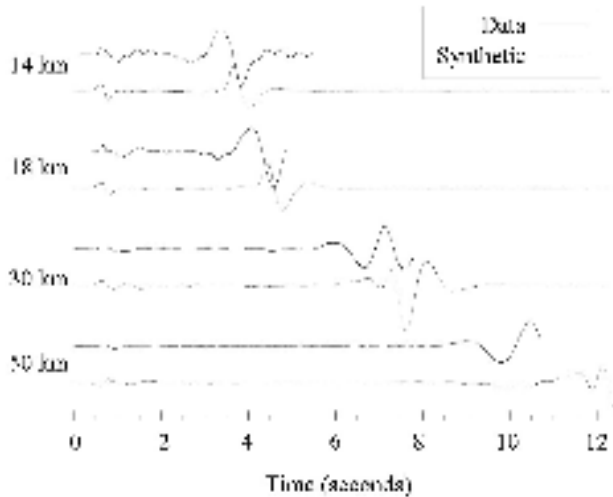

Figure 4. Synthetic and observed seismograms for the 1987/07/17 event. Synthetics were created using wavenumber integration and were low pass filtered at 2 Hz.
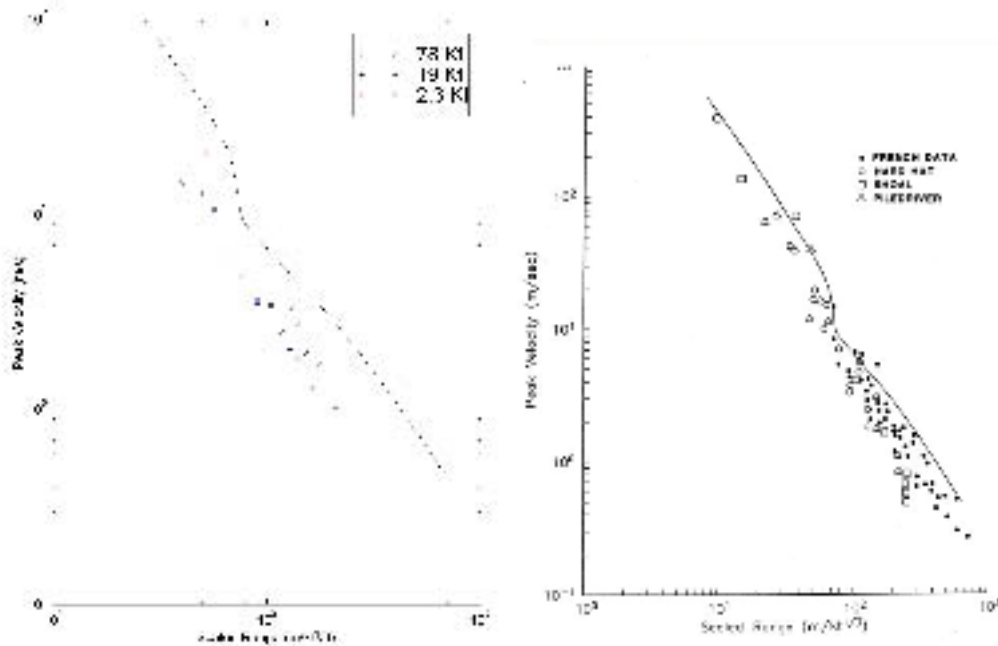

Figure 5. Peak velocity vs. scaled range for the first three Degelen explosions (left) and for historic data from U.S. and French explosions. The solid line is the prediction from the PILEDRIVER simulation discussed in the next section and shown earlier in Figure 1. The Degelen velocities are near the lower bound of the historic data set.

Numerical Modeling of Explosions

The parameters used in numerical simulations of underground nuclear explosions are constrained by laboratory material properties tests and by direct observations of ground motion from underground explosions. Laboratory measurements of strength for brittle hardrocks seem to be very inconsistent with *insitu* strength as inferred by modeling of underground explosions. In particular, finite difference calculations of ground motion in granite, made using the laboratory measurements of shear strength, have invariably given much narrower particle velocity pulses and much smaller displacements than those measured in the field. Constitutive models have been developed (Rimer and Lie, 1982, Rimer, et al., 1984) which attribute this weaker behavior of *insitu* granite and other rocks under explosive loading to ground-motion-induced rock damage or pore fluid pressure increases. Comparisons have already been made in Figure 1 between the particle velocity measurements at working point depth from the 62 kt PILEDRIVER event and the results of the pile570 numerical simulation, made using the effective stress model discussed in Rimer, et al (1984). Numerical results from pile570 are also in good agreement with the measured cavity radius and with the estimated seismic source function given in Table 2.

Table 2. United States Explosions in Granite

Explosion	Yield (kT)	Measured Cavity Radius (m)	Calculated (570) Cavity Radius (m)
PILEDRIVER	62.0	40.1/44.5	42.5
HARDHAT	5.9	19.4	19.4
SHOAL	12.5	26.8	24.9

For this simulation, effective stress model parameters were calibrated to best match the velocity peak and pulse shape at the closest-in gauge station (B-SL). This required a rapid buildup of pore pressure during the loading, leading to a large strength reduction very near the propagating shock front. Note that the pulse shapes at all four stations are rather consistent, with all including a long duration shallow negative velocity pulse. The peak velocities at the two smallest ranges agree very well with the simulation, but the measured peaks at the two larger ranges are a factor of two or more lower than the calculated peaks. The two closest PILEDRIVER gauges were located along roughly a 180 degree different azimuth than the other more distant gauges. However, a connection between possible site anisotropies and the measured ground motions has never been established. It should be noted that the 5.9 kt HARDHAT event, which was detonated in similar rock, near the later PILEDRIVER event, but at a shallower depth of burial, gave particle velocity pulses that were more similar to the PILEDRIVER pulses at the larger ranges. (See Rimer, Stevens, and Day, 1987, for a comparison between the results of the pile570 simulation and the HARDHAT measurements.)

The constitutive models used in these simulations are phenomenological in nature and do not explicitly account for the dynamic response of the *insitu* fractures in the crystalline rock. The Sammis micro-mechanical damage model for brittle rocks under compressive loading (see Ashby and Sammis, 1990) has been incorporated into our numerical simulation codes. This model introduces a damage parameter, related to the increase in flaw size from its pre-shot average value. Damage accumulates as the flaws extend during the compressive loading and reaches some maximum value at which the rock fails unstably. Since unstable compressive failure of a rock element is calculated using this model to occur relatively early in the dynamic motions of interest here, i.e., usually near the propagating shock front, additional modeling was incorporated to complete the description of the stress field after this failure. Limiting the magnitude of deviatoric stresses in a failed rock element through the use of a standard friction law was shown to not provide sufficient strength reduction to simulate the ground motion measurements. In particular, calculated particle velocity time histories were still much narrower than the measured pulses for all reasonable choices of initial flaw size.

The additional strength reduction required to sufficiently broaden the particle velocity pulses was obtained by using a shear damage model originally developed for soft rocks such as tuff, described in Rimer and Proffer (1991). As discussed in Rimer et al (1999), this shear damage model was applied here only for rock elements that had experienced the onset of unstable compressive failure. Thus, a rock element was allowed to undergo significant damage before application of this treatment. The post-failure shear damage model performs an interpolation between the standard coefficient of friction of 0.60 and much lower "effective

friction" values of 0.02-0.20 in the friction law used to limit deviatoric stresses. This linear interpolation is based on the maximum shear strain experienced by the failed rock element.

A series of calculations were made using the Sammis modeling, quantifying the effect of model parameters on particle velocity pulse shapes, cavity radius, and RDP. Calculated particle velocity pulse widths were sensitive to the choice of shear strain magnitude required for full strength reduction, with lower values of this parameter resulting in longer pulse duration and larger RDP. The simulation which best fits all of the PILEDRIVER ground motion data is Run PD10. Comparisons with measured particle velocities are shown in Figure 6. In contrast with the results of pile570, Figure 1, made with the effective stress model, PD10 provides a much better fit to the PILEDRIVER data at the two larger ranges, while underestimating peak velocities at the closest ranges. Subsequent analyses showed that the timing of the strength reductions for the two models were somewhat different, with the effective stress model providing an earlier reduction than the present damage model. However, calculated cavity radius and RDP with the new model are in as good agreement with the measurements as were those with the effective stress model. It is important to emphasize that while the shear damage model (or some other post-failure strength reduction model) is crucial to successful simulation of the ground motion data, it is the micro-mechanical damage mechanics model that primarily determined the size of the central core of low strength rock around the cavity.
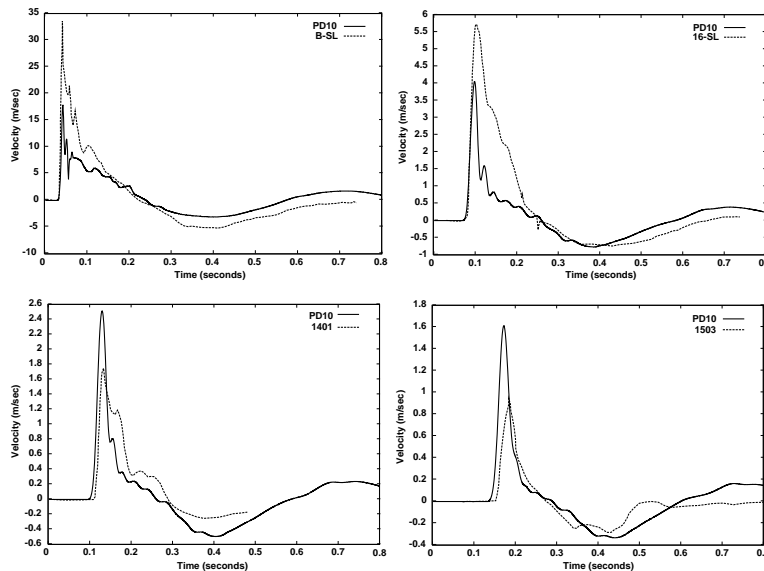

Figure 6. Calculated particle velocity pulses at four ranges for Run PD10 and PILEDRIVER measurements

Acoustic Fluidization

A possible physical mechanism for the strength reduction and very low coefficients of friction discussed in the previous section is the "acoustic fluidization" concept proposed by Melosh (1979) to explain the low strengths (or very low angles of internal friction) apparent in a number of geologic processes, such as seismic faulting, impact crater slumping, and long runout landslides. The main concept of this proposed mechanism is that "sufficiently strong acoustic waves in rock debris can momentarily relieve the static overburden in limited regions of the rock mass, thus allowing sliding to occur in the unloaded region. If this happens frequently enough, flow of the entire rock mass results." In terms of the explosively-induced ground motions of interest here, only the mass of failed or fractured rock would have the potential for acoustic fluidization. The dynamic fracturing process, by itself, provides enough energy to generate sufficiently strong oscillations post-failure to reduce the "effective normal stress/effective friction" to the low values required in the weak core region near the cavity.

We are implementing an approximate representation of acoustic fluidization within our nonlinear finite difference code and have applied it to simulation of PILEDRIVER. Two different schemes are being

implemented, both of which have the following characteristics in common: 1) Acoustic fluidization occurs only after failure has occurred in the cell, and 2) Acoustic fluidization is related to the kinetic energy of each cell. So the basic assumptions of the calculation are that once a cell has failed, it is subject to acoustic fluidization, and that the acoustic fluidization occurs only after the kinetic energy reaches some critical threshold level. The second assumption is not quite right – acoustic fluidization is related to acoustic vibrations within each cell, but it is reasonable to expect these vibrations to be approximately related to the kinetic energy of the cell. We also introduce a decay constant to simulate the decaying acoustic vibrations

in each cell that satisfies the equation $\tau \dfrac{d\theta}{dt} + \theta = \dfrac{\rho v^2}{2}$

where τ is the decay time, ρ is density, v is particle velocity, and θ is the kinetic energy. Acoustic fluidization occurs if θ exceeds a threshold level in the rubbleized cell. The effect of this equation has been shown in preliminary calculations to: 1) by delaying the onset of θ, smooth the large strength reduction introduced by acoustic fluidization (and to smooth the velocity pulses), and 2) slow the rapid decrease in θ at the end of the step function. An additional modification has been introduced recently to allow the onset and decay times to occur at different rates, since it was found that the equation above causes too long a delay in onset time. In the example below, we discuss only the case for $\tau=0$ which corresponds to an instantaneous onset time and abrupt stoppage of acoustic fluidization. Additional calculations with varying onset and decay rates are currently being conducted.

 Implementation 1 – Failure and acoustic fluidization defined by damage model

First-principles implementation of the strong vibrational mode of the acoustic fluidization mechanism is beyond the capabilities of the finite difference continuum code that computes the ground motion. However, we have included some of the observed phenomenological features of the acoustic fluidization mechanism in our computational model. Application is restricted to rock elements that have both previously been reduced to rubble (using the Sammis brittle failure model) and been driven to a sufficiently large kinetic energy. These rock elements are then assigned lower shear strengths through the use of a reduced effective pressure or an increased "acoustic fluidization pressure" in the standard friction law.

We implement this mechanism in terms of the specific kinetic energy density ($\rho v^2 / 2$) level, called Ek. When this kinetic energy goes above some threshold level, Afonke, acoustic fluidization occurs and the effective pressure consequently drops down. In the finite difference code, the effective pressure field is given by $P_{acf}=P-P_f$, where P is pressure and P_f is the acoustic fluidization induced pressure.

The stress difference, $Y=b* P_{acf}$, is related to Pacf using a friction law where b is the friction coefficient. We assume that acoustic fluidization induced pressure is proportional to both pressure and the kinetic energy density in the mass element through the relation, $P_f=Ek/Afkemx *P$, where Afkemx is a normalization factor. The effective pressure Pacf would drop to zero if the kinetic energy is greater than afkemx. Note that P_f decreases as the particle velocity and kinetic energy in a cell become smaller behind the shock front. Thus, the strength reduction due to acoustic fluidization decreases with time in the cell.

This section contains finite difference simulations of the PILEDRIVER explosions that were made to evaluate both the Sammis micro-mechanical damage mechanism model and the acoustic fluidization mechanism by comparing synthetics and observations. We start first with a series of runs, aiming to find the best parameters, afonke, afkemx, according to the above mechanism, to approximate the observations.

Table 3 shows results such as failure extent, damage extent, acoustic fluidization extent, final cavity size (Rc) and maximum cavity size and RDP different combinations of the two parameters, afonke and afkemx. We notice that the final scenarios are quite sensitive to these parameters, and generally the greater value of afonke and afkemx corresponds to the smaller damage zone and smaller failure zone. We find that the combination Afonke=afkemx=1e6 (erg/cm^3) (Case Pa04 in Table 3) better fits the cavity size and RDP for PILEDRIVER. The particle motion observations and synthetics with this combination of parameters at four locations are shown in Figure 7.

Table 3 Parametric studies of acoustic fluidization.

| RUN-ID	Afonke (erg/cm^3)	Afkemx (erg/cm^3)	Failure extent (m) (ifdam=4)	Damage extent (m) (ifdam=1)	Extent of A.F. (m)	Rc (final) (m)	Rcmax (m)	RDP, phi (10^3 m^3)
Pa03	1e6	1e7	367.6	552.4	212.2	47.391	48.31	23
Pa04	1e6	1e6	436.8	630.1	212.2	42.748	56.95	16
Pa05	1e6	5e6	394.1	590.1	212.2	50.045	51.19	26
Pa06	1e6	2e6	436.8	609.8	220.6	49.202	54.98	25
Pa09	1e7	1e7	367.6	552.4	129.0	46.457	47.19	21
Pa10	1e5	1e7	367.6	552.4	342.7	47.480	48.40	22
Pa11	2e5	1e6	451.9	630.1	319.2	43.090	58.49	17
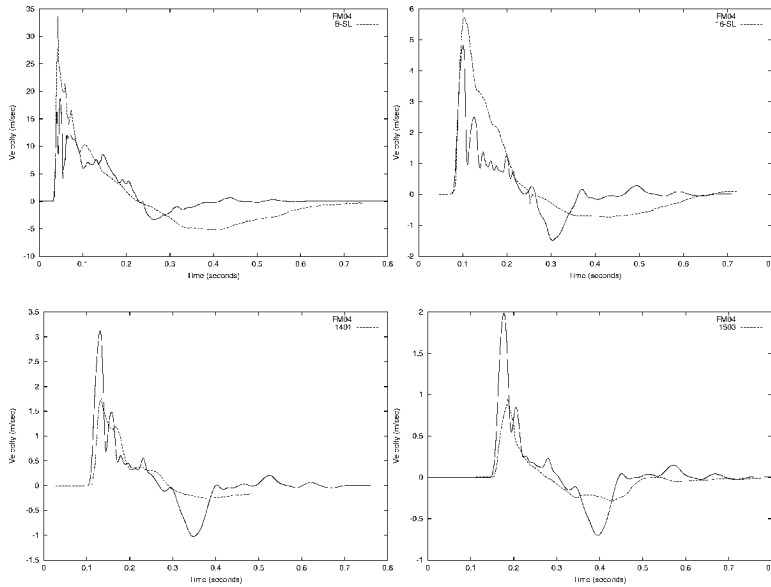
Figure 7. Comparison between observations (dashed lines) and synthetics (solid lines) made with acoustic fluidization. afonke=afkemx=10^6 erg/cm^3.

The simulated waveforms shown in Figure 7 match some of the characteristics of the measured waveforms but are not as good a fit to the data as were those shown earlier in Figure 1 (for the effective stress model) or Figure 6 (for the Sammis model augmented by a post-failure shear damage model). In particular, the very simple model for acoustic fluidization outlined above results in larger negative pulse amplitudes and shorter negative pulse durations than those measured. Part of this is due to a problem in the implementation – as velocity changes from positive to negative the kinetic energy reaches zero and acoustic fluidization abruptly turns off, which is clearly incorrect. Introduction of a decay time into the above acoustic fluidization algorithm to correct this problem has shown the potential for increasing negative pulse durations and bringing the acoustic fluidization results into better agreement with the measurements.

However, the noise in the waveforms produced using the Sammis brittle failure model (Figures 6 and 7) is a consequence of the large strength reduction for failed rock compared to the elastic (infinite strength) deviatoric behavior required for compatibility with the model in the damaged rock outside of it. (See Rimer, et al, 1999, for a discussion of the effects of numerical smoothing of the discontinuity between failed and damaged rock elements for the PD10 model.)

Implementation 2 – Failure and start of acoustic fluidization defined by laboratory strength model, followed by plastic flow

The simulations described in the previous section are noisy, in large part due to incompatibilities both between the brittle failure model and possible plastic behavior near the explosive source and between the elastic pressure-volume relation for undamaged rock and the nonlinear loading relation measured on small samples of granite in the laboratory. In order to incorporate these nonlinear rock behaviors, we removed the Sammis model and instead used the laboratory failure surface for damaged granite as the trigger point for

acoustic fluidization. Calculations were run with this failure surface and the polynomial EOS for granite developed from compressive loading tests on Piledriver rock samples. We assume plastic yielding and a non-associated flow rule (radial return) and use the plastic work (epw) done on a rock element as the threshold to determine if the cell is rubbleized (to initiate the acoustic fluidization model). The acoustic fluidization threshold is set to the same value as implementation #1. These calculations are in progress.

CONCLUSIONS AND RECOMMENDATIONS

IDG is in the process of digitizing data from 25 nuclear tests at the Degelen test site. The complete data set consists of 81 near field waveforms recorded underground at shot depth and 124 (unique) near regional seismic records. IDG has digitized 27 near field waveforms and 122 seismic waveforms (including multiple records of the same signal), and will complete digitization of the remainder of the data set over the duration of this project. The data set of near field and regional waveforms will be delivered to the Center for Monitoring Research upon completion of this project.

We are in the process of defining the optimum procedures to model this data. The goal is to develop material models that are consistent with the data and have a realistic physical basis. Work to date at SAIC has focused on implementation and testing of improved numerical modeling procedures and simulation of near regional data. We are testing acoustic fluidization as a physical mechanism for strength reduction in nonlinear explosion simulations. Preliminary results are promising, but additional work is required to improve the realism of the models. This initial study has focused on modeling of the PILEDRIVER data set with new material models. During the next year, we will continue this modeling effort and also focus on modeling the Degelen data set. Near field data will be modeled with our nonlinear finite difference code as described in this report with improved material models. Near regional data will be modeled using wave number integration.

REFERENCES

Ashby, M.F. and C.G. Sammis (1990), "The Damage Mechanics of Brittle Solids in Compression," *PAGEOPH*, Vol. 133, No. 3.

Luco, J. E. and R. J. Apsel (1983), "On the Green's functions for a layered half-space. Part 1.," *Bull. Seism. Soc. Am.*, 73, 909-929.

Melosh, H.J. (1979), "Acoustic Fluidization: A New Geologic Process?," *J. Geophys. Res.*, 84, 7513, December.

Melosh, H.J., and B.A. Ivanov (1999), "Impact Crater Collapse," *Annual Rev. Earth Planet Science*, 27, pp385-415.

Rimer, N. and K. Lie (1982), "Numerical Simulation of the Velocity Records from the SRI Grout Spheres Experiments," S-CUBED Topical Report DNA-TR-82-54, September.

Rimer, N., S. M. Day, G. A. Hegemier, H. E. Read, S. K. Garg, and S. Peyton (1984), "Effect of Pore Fluid Pressure on Explosive Ground Motions in Low Porosity Brittle Rocks," DNA-TR-85-245, July.

Rimer, N., J. L. Stevens, and K. H. Lie (1986), "Effects of Pore Pressure and Fractures on Ground Motion in Granite," S-CUBED Final Report DNA-TR-86-227, June.

Rimer, N., J. L. Stevens, and S.M. Day (1987), "Effects of Pore Pressure, Fractures, and Dilatancy on Ground Motion in Granite," S-CUBED Final Report AFGL-TR-87-0136, April.

Rimer, N. and W. Proffer (1991), "Containment Phenomenology Using a New Shear-Strain-Based Computational Damage Model for Tuff," S-CUBED Report SSS-DTR-91-12612, September.

Rimer, N., K. Lie, J.L. Stevens, J.R. Murphy, and G.G. Kocharyan (1998), "A Micro-Mechanical Damage Model for Estimating Seismic Source Characteristics of Underground Explosions in Hardrock," Maxwell Technologies Technical Report MFD-DTR-98-15985, January.

Rimer, N., J.L. Stevens, J.R. Murphy, and G.G. Kocharyan (1999), "Estimating Seismic Source Characteristics of Explosions in Hardrock Using a Micro-Mechanical Damage Model," Maxwell Technologies Final Report MTSD-DTR-99-16423, July.

Stevens, J. L. (1986), "Estimation of scalar moments from explosion-generated surface waves," *Bull. Seism. Soc. Am.*, v. 76, pp. 123-151.

Stevens, J. L., N. Rimer, and S. M. Day (1986), "Constraints on modeling of underground explosions in granite," S-CUBED annual report, AFGL-TR-86-0264, SSS-R-87-8312, October.